scientific reports

OPEN

Prominent luminescence of silicon-vacancy defects created in bulk silicon carbide p–n junction diodes

Fumiya Nagasawa✉, Makoto Takamura, Hiroshi Sekiguchi, Yoshinori Miyamae, Yoshiaki Oku & Ken Nakahara

We investigate fluorescent defect centers in 4H silicon carbide p–n junction diodes fabricated via aluminum-ion implantation into an n-type bulk substrate without the use of an epitaxial growth process. At room temperature, electron-irradiated p–n junction diodes exhibit electroluminescence originating from silicon-vacancy defects. For a diode exposed to an electron dose of 1×10^{18} cm^{-2} at 800 keV, the electroluminescence intensity of these defects is most prominent within a wavelength range of 400–1100 nm. The commonly observed D_1 emission was sufficiently suppressed in the electroluminescence spectra of all the fabricated diodes, while it was detected in the photoluminescence measurements. The photoluminescence spectra also displayed emission lines from silicon-vacancy defects.

The silicon-vacancy (V_{Si}) defect in silicon carbide (SiC) is currently one of the most promising fluorescent defect centers for industrial applications. Applications of this defect have been widely proposed, including magnetic and/or temperature sensors[1–5], qubits[6,7], single photon emitters[8], and microwave emitters[9]. Industrial and academic interest have promoted research on the diamond nitrogen-vacancy center[10] for several decades. However, the V_{Si} defect in SiC has several advantages compared to diamond, including the mature process technology and material availability of SiC owing to the recent success of SiC power devices.

From an industrial point of view, the high manufacturing cost of SiC power devices[11] hinders the industrialization of V_{Si}-based SiC devices. Because SiC epitaxy is one of the most expensive processes involved in manufacturing these devices[12], a wafer structure without epitaxial layers is preferable. Another crucial issue concerns the excitation method of V_{Si} defects. Optical excitation has been used in a number of reported experiments[2–9]. However, this method requires an additional optical pumping source and fine optical alignment, consequently leading to high costs. Electrical excitation, conversely, is mandatory in practice because it simplifies the system. To the best of our knowledge, no electroluminescence (EL) measurements of V_{Si} defects in bulk SiC have yet been reported. However, several groups have reported EL measurements of color centers in epitaxial SiC films[13–16]. All such results show a two-color spectrum, indicating the inevitable generation of several types of luminescent defects. Multiple-color emissions are not acceptable in practice because of the resulting inefficient excitation of specific color centers. The commonly observed, but always unintentionally introduced, emission band stems from the so-called D_1 center[17], which is associated with a silicon antisite (Si_C) defect. The suppression of the D_1 emission band in EL spectra is therefore of great importance to realize V_{Si}-functional devices.

In this study, we used a commercially available n-type 4H-SiC substrate, i.e., one that is widely used for power devices, to fabricate p–n junction diode structures. The p-type region was formed via aluminum (Al) ion implantation instead of p-SiC epitaxy. V_{Si} defects were generated in the SiC substrate via electron irradiation. The luminescence was measured using both electrical and optical excitation methods. The experimental results demonstrate that V_{Si}-originated emission dominates the EL spectra, while other emissions, e.g., D_1 center-related emission, are negligible.

Rohm Research and Development Center, ROHM Co., Ltd., Kyoto, Japan. ✉email: fumiya.nagasawa@dsn.rohm.co.jp

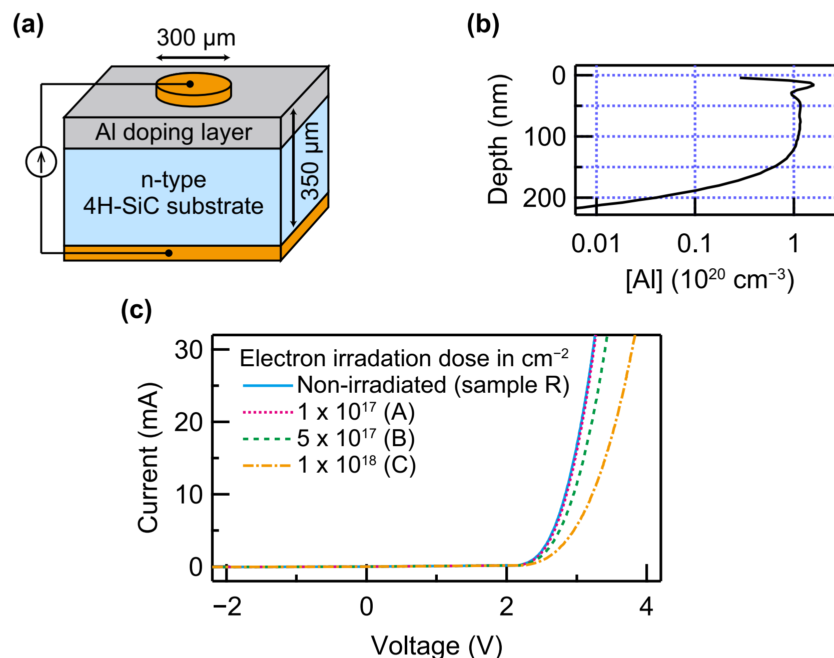

Figure 1. p–n junction diode in a bulk 4H-SiC substrate. (**a**) Schematic of a fabricated p–n junction structure. The nitrogen concentration in the n-type SiC substrate is on the order of 10^{19} cm^{-3}. A p-type layer was formed via the multistep implantation of Al ions. (**b**) Depth profile of the Al concentration, [Al]. In the flat-profile region, [Al] exceeds the nitrogen concentration. (**c**) Current–voltage characteristics of the samples with an electron irradiation dose of 0 (sample R), 1×10^{17} (A), 5×10^{17} (B), and 1×10^{18} cm^{-2} (C). An increase in the electrical resistance is observed for the high-irradiation-dose samples.

Results and discussion

Figure 1a shows the sample structure fabricated in this study. A single p–n junction was formed via Al-ion implantation into an n-type 4H-SiC substrate followed by annealing at 1650 °C. A simulated Al concentration[18] in a doping layer is shown in Fig. 1b. Electron irradiation at the energy of 800 keV was performed to introduce intrinsic defects. We prepared four groups of samples with different irradiation doses (sample A: 1×10^{17} cm^{-2}, B: 5×10^{17} cm^{-2}, C: 1×10^{18} cm^{-2}, and R: non-irradiated reference). The current–voltage characteristics of all the samples are shown in Fig. 1c. A higher electron-irradiation dose increases the electrical resistance. We attribute such an increase to the generation of the non-radiative recombination centers of $Z_{1/2}$ and $EH_{6/7}$[19]. The high nitrogen concentration in the substrate prevented the samples from reached a semi-insulating state.

Figure 2 shows the room-temperature EL spectra at a driving current of 20 mA. As can be seen in Fig. 2, sample R shows a broad emission band around 720 nm. In addition to this band, another emission band with a peak wavelength at 910 nm appeared for samples A, B, and C. The emission at 910 nm is a characteristic of V_{Si} defects[21]. The V_{Si}-related emission dominates the spectra of samples A, B, and C. In particular, for sample C, it exceeds the other emission peaks by a factor of 11. Conversely, the V_{Si} emission is negligibly small for sample R. Because the post-implantation annealing temperature of 1650 °C was sufficiently higher than the anneal-out temperature of the V_{Si} defects, i.e., 750 °C[22], the V_{Si} concentration introduced by the Al-ion implantation was significantly reduced during the annealing process. Therefore, the V_{Si} defects in samples A, B, and C were generated purely via the electron irradiation.

Figure 3 shows the integrated intensity of the V_{Si} emission as a function of the injection current I. Saturated behavior for large I is observed for samples A, B, and C. The fit of the equation[23] $P \propto (1 + I_0/I)^{-1}$, where P is the EL integrated intensity and I_0 is the saturation current, yields $I_0 = 13.7$ mA for sample C. This value is larger than the value of $I_0 = 5.3$ mA for the nitrogen-vacancy-related EL of diamond[24] but comparable to the value of $I_0 = 10$ mA for the V_{Si}-related EL of 6H-SiC[13].

We now turn to the 720 nm band observed in the EL spectra in Fig. 2. The origin of this band seems neither carbon antisite–vacancy pair ($C_{Si}V_C$) defects[25,26] nor D_1 defects, but annealing-related defects[20]. The $C_{Si}V_C$ defect is reported to completely disappear with high-temperature annealing around 1100 °C[26] which is much lower than the employed annealing temperature. In addition, their zero-phonon lines, AB lines[25,26], were not detected in the photoluminescence (PL) measurements at 10 K (see Supplementary Fig. S1a online). Regarding the D_1 defects, the annealing out of them should not occur in our experiments because these defects are thermally stable up to 1700 °C[27]. However, although the D_1 emission intensity should increase with electron irradiation[28], Supplementary Fig. S2 shows that their EL intensity is not affected by electron irradiation. Thus, there is no good reason to attribute the 720 nm band to $C_{Si}V_C$ or D_1 defects. The annealing-related defects may be the origin of this band, however, their varied emission wavelength for each defect[20] makes further identification difficult.

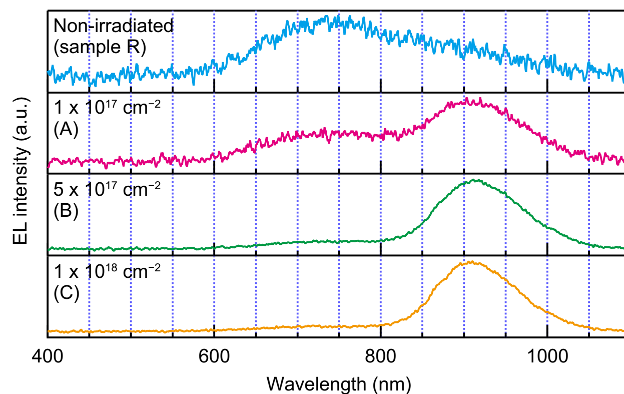

Figure 2. Electroluminescence (EL) spectra at a temperature of 300 K. All measurements were performed at a bias current of 20 mA. Labels in each panel indicate the conditions of the electron irradiation dose. Note that the vertical scales are different for each panel. An emission peak around 910 nm, originating from the silicon-vacancy defects, appears with electron irradiation. This emission dominates the EL spectrum for the electron-irradiated samples (A, B, and C). The broad emission band around 720 nm is attributed to the annealing-related defects[20]. D_1 luminescence was not observed.

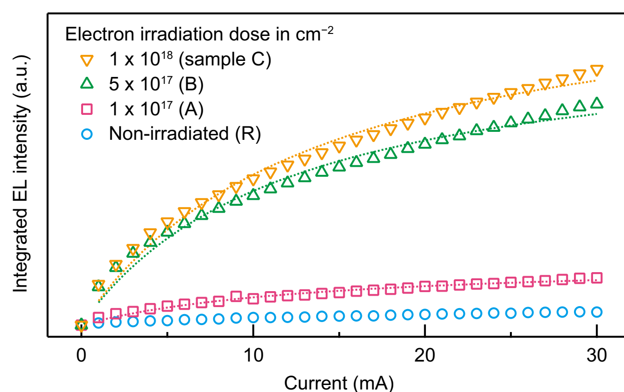

Figure 3. Current dependence of the integrated electroluminescence (EL) intensity for the 910 nm emission band. The integration range is fixed to 910 ± 60 nm. Saturation of the integrated EL intensity is observed for the irradiated samples (A, B, and C). Dotted lines represent fits using the saturation-curve equation[23].

In the following, we discuss plausible mechanisms underlying the absence of D_1-originated EL. Unlike the EL measurements, the D_1 emission was observed in the PL measurements for samples R and C even at room temperature, and was not observed in a bare SiC substrate (see Supplementary Fig. S1b online). Therefore, D_1 defects were introduced at least to the penetration depth of excitation light from the top-surface via Al-ion implantation and electron irradiation. Based on the above results, the deteriorated crystal quality in the vicinity of the p–n junction by the high-fluence implantation of Al ions may be the mechanism of the smeared D_1 band in all of the EL spectra. It has been established that variations in the stacking faults of SiC are sensitive to the wavelength of the D_1-emission line[14]; therefore, this interpretation is reasonable. According to this mechanism, our EL results suggest that D_1 defects are more sensitive to the crystal quality than V_{Si} because V_{Si}-related EL can still be observed in the electron-irradiated, i.e., additional defect-introduced, samples. Also, defect diffusion is another possible mechanism. The depth profile of Al-implanted 4H-SiC, as detected by cathode luminescence[29], revealed that high-temperature annealing induces the diffusion of D_1 defects from the surface-implanted area, with a diffusion length of up to several micrometers, while the implanted Al atoms remain in the vicinity of the surface. The low concentration of D_1 defects in the p–n junction layer then would result in the absence of D_1 -related EL. This mechanism, however, leaves an open question as to why the D_1-emission band does not appear after electron irradiation (see Supplementary Fig. S2 online); electron irradiation should generate the D_1 defects[28]. Lastly, note, thermal activation of the defect-bound electrons in the conduction band[13] due to current injection is not the mechanism of the absence of D_1 EL, because the comparison of the EL spectra between the smallest ($I = 1$ mA) and largest (30 mA) currents revealed that there was no significant difference in the shape of EL spectra and the D_1 EL was not detected for the both currents (see Supplementary Fig. 3 online).

The PL spectra of samples R and C with a 785-nm excitation laser are shown in Fig. 4. Except for the Raman scattering peaks of 4H-SiC at 836 nm and 850 nm[30], as shown in the upper panel of Fig. 4a, no significant emission

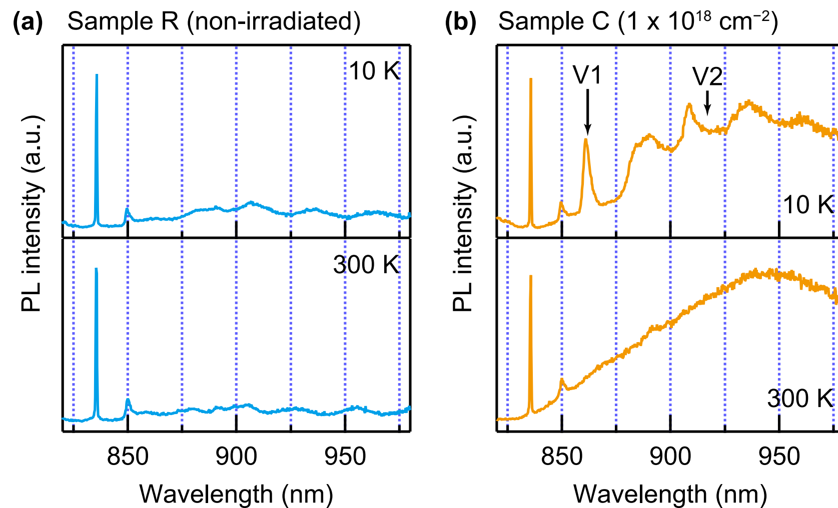

Figure 4. Photoluminescence (PL) spectra with a 785-nm excitation laser at room temperature. The excitation energy is 3.7 mW at the top surface of the samples. The PL spectrum for the (a) non-irradiated and (b) 1×10^{18} cm^{-2}-irradiated samples. Measurements were performed at temperatures of 10 K (upper panel) and 300 K (lower panel). The V_1 zero-phonon line of the silicon-vacancy defects is clearly seen at 10 K for the irradiated sample. The emission lines at 836 nm and 850 nm originate from the Raman scattering of 4H-SiC[30].

peaks were observed for sample R at 10 K. As can be seen in the lower panel of Fig. 4a, the PL spectrum at 300 K does not show a large difference. These results indicate the absence of V_{Si} defects in sample R. Conversely, as shown in the upper panel of Fig. 4b, the 862-nm emission line, labeled V1, appears in the PL spectrum of sample C at 10 K. This emission line originates from the V_1 zero-phonon line of the V_{Si} defects in 4H-SiC[31]. The V_2 emission line at 917 nm was too weak to be assigned compared to the large phonon sideband (PSB), which corresponds to the large Huang–Rhys (HR) factor (the small Debye–Waller factor[32]). Note, V'_1 line, which is associated with a second excited state of the V_{Si} defect[33], was not detected possibly due to a low measurement temperature[31]. The 300-K PL spectrum of sample C in the lower panel of Fig. 4b shows a broad PSB originating from the V_{Si} defects with its peak wavelength around 940 nm, which is slightly longer than the typical wavelength for the V_{Si} PL. However, the PSB peak around 950 nm was observed with the experimental setup similar to ours[34], and is reasonable for the large HR factor. The discrepancy of the peak wavelength of the V_{Si}-related PSB between the EL and PL spectra is perhaps due to the different local crystalline structures under detection. Therefore, both the EL and PL measurements substantiate the feasibility of efficient V_{Si} luminescence emitted from a bulk SiC substrate with no epitaxial layers.

Conclusion

In conclusion, we successfully fabricated p–n junction diodes including V_{Si} defects on a bulk 4H-SiC substrate without epitaxial layers. The PL spectra demonstrated the formation of V_{Si} defects. The EL measurements revealed that the luminescence intensity of V_{Si} was most prominent within the measured wavelength range. Further, the commonly observed D_1 emission was sufficiently suppressed in the EL spectra, while it was detected in the PL measurements. The absence of the D_1 emission in the EL spectra suggests that the deteriorated crystal quality due to ion implantation affects its luminescence. Our approach provides a foundation for novel applications of V_{Si} defects in SiC using simple manufacturing processes.

Methods

We employed an n-type 4H-SiC substrate with a nitrogen concentration on the order of 10^{19} cm^{-3} purchased from SiCrystal AG. Multi-energy Al-ion implantation was performed at a substrate temperature of 500 °C to form a p-type region on the top-surface of the substrate. The fluence and energy values of the Al implantation were 2.0×10^{14}, 2.0×10^{14}, 2.5×10^{14}, 2.5×10^{14}, and 8.0×10^{14} cm^{-2} at 10, 30, 50, 70, and 100 keV, respectively. According to an SRIM-code simulation[18], the Al atoms should be flatly distributed from the surface to a depth of 130 nm with an Al concentration of 1×10^{20} cm^{-3}. Post-implantation annealing was performed at 1650 °C for 30 min in an argon atmosphere. Subsequent to annealing, the substrate was diced into chips. These chips were divided into four groups. The first three groups were irradiated with 800-keV electrons at doses of 1×10^{17} (sample A), 5×10^{17} (sample B), and 1×10^{18} cm^{-2} (sample C). The remaining group (sample R) was not irradiated by electrons and served as a reference. Finally, Ti/Ni/Au Schottky contact metal was deposited on the top and bottom surfaces of the chips via electron-beam evaporation. The top-surface electrodes were circularly shaped with a diameter of 300 μm.

Data availability

The data that support the findings of this study are available from the corresponding author on reasonable request.

Received: 24 September 2020; Accepted: 31 December 2020
Published online: 15 January 2021

References

1. Weber, J. R. *et al.* Quantum computing with defects. *Proc. Natl. Acad. Sci. U. S. A.* **107**, 8513–8518. https://doi.org/10.1073/pnas.1003052107 (2010).
2. Kraus, H. *et al.* Magnetic field and temperature sensing with atomic-scale spin defects in silicon carbide. *Sci. Rep.* **4**, 5303. https://doi.org/10.1038/srep05303 (2014).
3. Simin, D. *et al.* High-precision angle-resolved magnetometry with uniaxial quantum centers in silicon carbide. *Phys. Rev. Appl.* **4**, 014009. https://doi.org/10.1103/PhysRevApplied.4.014009 (2015).
4. Simin, D. *et al.* All-optical dc nanotesla magnetometry using silicon vacancy fine structure in isotopically purified silicon carbide. *Phys. Rev. X* **6**, 31014. https://doi.org/10.1103/PhysRevX.6.031014 (2016).
5. Niethammer, M. *et al.* Vector magnetometry using silicon vacancies in 4H-SiC under ambient conditions. *Phys. Rev. Appl.* **6**, 034001. https://doi.org/10.1103/PhysRevApplied.6.034001 (2016).
6. Riedel, D. *et al.* Resonant addressing and manipulation of silicon vacancy qubits in silicon carbide. *Phys. Rev. Lett.* **109**, 226402. https://doi.org/10.1103/PhysRevLett.109.226402 (2012).
7. Widmann, M. *et al.* Coherent control of single spins in silicon carbide at room temperature. *Nat. Mater.* **14**, 164–168. https://doi.org/10.1038/nmat4145 (2015).
8. Fuchs, F. *et al.* Engineering near-infrared single-photon emitters with optically active spins in ultrapure silicon carbide. *Nat. Commun.* **6**, 7578. https://doi.org/10.1038/ncomms8578 (2015).
9. Kraus, H. *et al.* Room-temperature quantum microwave emitters based on spin defects in silicon carbide. *Nat. Phys.* **10**, 157–162. https://doi.org/10.1038/nphys2826 (2014).
10. Manson, N. B., Harrison, J. P. & Sellars, M. J. Nitrogen-vacancy center in diamond: model of the electronic structure and associated dynamics. *Phys. Rev. B* **74**, 104303. https://doi.org/10.1103/PhysRevB.74.104303 (2006).
11. Status of the power electronics industry. Tech. Rep. (2019).
12. SiC market for power electronics. Tech. Rep. (2011).
13. Fuchs, F. *et al.* Silicon carbide light-emitting diode as a prospective room temperature source for single photons. *Sci. Rep.* **3**, 1637. https://doi.org/10.1038/srep01637 (2013).
14. Lohrmann, A. *et al.* Single-photon emitting diode in silicon carbide. *Nat. Commun.* **6**, 7783. https://doi.org/10.1038/ncomms8783 (2015).
15. Yamazaki, Y. *et al.* Electrically controllable position-controlled color centers created in SiC pn junction diode by proton beam writing. *J. Mater. Res.* **33**, 3355–3361. https://doi.org/10.1557/jmr.2018.302 (2018).
16. Sato, S. *et al.* Room temperature electrical control of single photon sources at 4H-SiC surface. *ACS Photonics* **5**, 3159–3165. https://doi.org/10.1021/acsphotonics.8b00375 (2018).
17. Castelletto, S. & Boretti, A. Silicon carbide color centers for quantum applications. *J. Physics: Photonics* **2**, 22001. https://doi.org/10.1088/2515-7647/ab77a2 (2020).
18. Ziegler, J. F., Ziegler, M. D. & Biersack, J. P. Srim—the stopping and range of ions in matter. *Nucl. Instrum. Methods Phys. Res. Sect. B Beam Interact. Mater. Atoms* **268**, 1818–1823. https://doi.org/10.1016/j.nimb.2010.02.091 (2010).
19. Kaneko, H. & Kimoto, T. Formation of a semi-insulating layer in n-type 4H-SiC by electron irradiation. *Appl. Phys. Lett.* **98**, 262106. https://doi.org/10.1063/1.3604795 (2011).
20. Lienhard, B. *et al.* Bright and photostable single-photon emitter in silicon carbide. *Optica* **3**, 768. https://doi.org/10.1364/OPTICA.3.000768 (2016).
21. Hain, T. C. *et al.* Excitation and recombination dynamics of vacancy-related spin centers in silicon carbide. *J. Appl. Phys.* **115**, 133508. https://doi.org/10.1063/1.4870456 (2014).
22. Itoh, H. *et al.* Photoluminescence of radiation induced defects in 3C-SiC epitaxially grown on Si. *J. Appl. Phys.* **77**, 837–842. https://doi.org/10.1063/1.359008 (1995).
23. Kurtsiefer, C., Mayer, S., Zarda, P. & Weinfurter, H. Stable solid-state source of single photons. *Phys. Rev. Lett.* **85**, 290–293. https://doi.org/10.1103/PhysRevLett.85.290 (2000).
24. Mizuochi, N. *et al.* Electrically driven single-photon source at room temperature in diamond. *Nat. Photonics* **6**, 299–303. https://doi.org/10.1038/nphoton.2012.75 (2012).
25. Steeds, J. W. Photoluminescence study of the carbon antisite-vacancy pair in 4H- and 6H-SiC. *Phys. Rev. B* **80**, 245202. https://doi.org/10.1103/PhysRevB.80.245202 (2009).
26. Castelletto, S. *et al.* A silicon carbide room-temperature single-photon source. *Nat. Mater.* **13**, 151–156. https://doi.org/10.1038/nmat3806 (2014).
27. Egilsson, T., Henry, A., Ivanov, I. G., Lindström, J. L. & Janzén, E. Photoluminescence of electron-irradiated 4H-SiC. *Phys. Rev. B* **59**, 8008–8014. https://doi.org/10.1103/PhysRevB.59.8008 (1999).
28. Lebedev, A. A., Ber, B. Y., Seredova, N. V., Kazantsev, D. Y. & Kozlovski, V. V. Radiation-stimulated photoluminescence in electron irradiated 4H-SiC. *J. Phys. D Appl. Phys.* **48**, 485106. https://doi.org/10.1088/0022-3727/48/48/485106 (2015).
29. Mitani, T., Hattori, R. & Yoshikawa, M. Depth profiling of Al ion-implantation damage in SiC crystals by cathodoluminescence spectroscopy. vol. 600, 615–618, https://doi.org/10.4028/www.scientific.net/MSF.600-603.615 (Trans Tech Publications Ltd, 2009).
30. Tunhuma, S. M. *et al.* Defects in swift heavy ion irradiated n-4H-SiC. *Nucl. Instrum. Methods Phys. Res. Sect. B Beam Interact. Mater. Atoms* **460**, 119–124. https://doi.org/10.1016/j.nimb.2018.11.046 (2019).
31. Wagner, M. *et al.* Electronic structure of the neutral silicon vacancy in 4H and 6H SiC. *Phys. Rev. B* **62**, 16555–16560. https://doi.org/10.1103/PhysRevB.62.16555 (2000).
32. Lindner, S. *et al.* Strongly inhomogeneous distribution of spectral properties of silicon-vacancy color centers in nanodiamonds. *New J. Phys.* **20**, 115002. https://doi.org/10.1088/1367-2630/aae93f (2018).
33. Nagy, R. *et al.* Quantum properties of dichroic silicon vacancies in silicon carbide. *Phys. Rev. Appl.* **9**, 034022. https://doi.org/10.1103/PhysRevApplied.9.034022 (2018).
34. Sato, S. *et al.* Formation of nitrogen-vacancy centers in 4H-SiC and their near infrared photoluminescence properties. *J. Appl. Phys.* **126**, 083105. https://doi.org/10.1063/1.5099327 (2019).

Acknowledgements

F.N. and Y.M. would like to appreciate the members of Quantum Beam Science Research Directorate at QST for their hospitality. We thank E. Miyai and W. Kunishi for fruitful discussion. We also thank T. Kishimoto and H. Kashiwa for experimental aid.

Author contributions

F.N., M.T., H.S., and K.N. conceived the experiments, F.N. and H.S. conducted the experiments, F.N., M.T., Y.M., Y.O., and K.N. analysed the results. F.N. and K.N. wrote the manuscript. All authors reviewed the manuscript.

Competing interests

The authors declare no competing interests.

Additional information

Supplementary Information The online version contains supplementary material available at https://doi.org/10.1038/s41598-021-81116-8.

Correspondence and requests for materials should be addressed to F.N.

Reprints and permissions information is available at www.nature.com/reprints.

Publisher's note Springer Nature remains neutral with regard to jurisdictional claims in published maps and institutional affiliations.

Open Access This article is licensed under a Creative Commons Attribution 4.0 International License, which permits use, sharing, adaptation, distribution and reproduction in any medium or format, as long as you give appropriate credit to the original author(s) and the source, provide a link to the Creative Commons licence, and indicate if changes were made. The images or other third party material in this article are included in the article's Creative Commons licence, unless indicated otherwise in a credit line to the material. If material is not included in the article's Creative Commons licence and your intended use is not permitted by statutory regulation or exceeds the permitted use, you will need to obtain permission directly from the copyright holder. To view a copy of this licence, visit http://creativecommons.org/licenses/by/4.0/.

© The Author(s) 2021